



Membrane fouling mechanism of biofilm-membrane bioreactor (BF-MBR): Pore blocking model and membrane cleaning

Yi Zheng^a, Wenxiang Zhang^{a,*}, Bing Tang^a, Jie Ding^a, Yi Zheng^b, Zhien Zhang^c

^a School of Environmental Science and Engineering and Institute of Environmental Health and Pollution Control, Guangdong University of Technology, Guangzhou 510006, China

^b School of Environmental Science and Engineering, Southern University of Science and Technology, Shenzhen 518055, Guangdong Province, China

^c School of Chemistry and Chemical Engineering, Chongqing University of Technology, Chongqing 400054, China

ARTICLE INFO

Keywords:

Biofilm membrane bioreactor (BF-MBR)
Filtration performance
Membrane fouling
Blocking model
Membrane cleaning

ABSTRACT

Biofilm membrane bioreactor (BF-MBR) is considered as an important wastewater treatment technology that incorporates advantages of both biofilm and MBR process, as well as can alleviate membrane fouling, with respect to the conventional activated sludge MBR. But, to be efficient, it necessitates the establishment of proper methods for the assessment of membrane fouling. Four Hermia membrane blocking models were adopted to quantify and evaluate the membrane fouling of BF-MBR. The experiments were conducted with various operational conditions, including membrane types, agitation speeds and transmembrane pressure (TMP). Good agreement between cake formation model and experimental data was found, confirming the validity of the Hermia models for assessing the membrane fouling of BF-MBR and that cake layer deposits on membrane. Moreover, the influences of membrane types, agitation speeds and transmembrane pressure on the Hermia pore blocking coefficient of cake layer were investigated. In addition, the permeability recovery after membrane cleaning at various operational conditions was studied. This work confirms that, unlike conventional activated sludge MBR, BF-MBR possesses a low degree of membrane fouling and a higher membrane permeability recovery after cleaning.

1. Introduction

A membrane bioreactor (MBR), combining membrane module and bioreactor, has been widely used for municipal and industrial wastewater treatment on account of high pollutant removal efficiency, better effluent quality, low sludge production rate and small footprint (Fenu et al., 2010; Ng and Kim, 2007). However, the serious membrane fouling, inefficient denitrification effect, and high operational cost limit its further application (Huang and Lee, 2015; Wang et al., 2014). Moving bed biofilm bioreactors (MBBR), as a kind of biofilm wastewater treatment technology, has been developed based on a combination of biological contact oxidation and biological fluidized bed and has been proved to be reliable for organic matter and nutrients degradation (Bassin et al., 2012; Luostarinen et al., 2006). Owing to high biomass and diversity in bacterial population, MBBR has some advantages, including stable and reliable operation, strong resistance to shock loading and adaptability, low residual sludge production and high nitrification rate (Bing et al., 2016; Leyva-Díaz et al., 2014). Biofilm membrane bioreactor (BF-MBR), as an alternative way, aimed at alleviating the fouling concerns in relation to MBR and the settle ability issues

regarding MBBR, and was proposed by Leiknes and Ødegaard (Ivanovic and Leiknes, 2012; Leiknes and Ødegaard, 2007).

In BF-MBR, membrane module and carriers are installed with a fixed or fluidized state. Membrane can trap macromolecular substances and solid particles, thus sustain high biomass concentration and bring about good pollutant degradation. At the same time, carriers have a large surface space, which is beneficial for microbial growth and pollutant degradation. Compared with the conventional activated sludge MBR, most of biomass in BF-MBR adhere to the surface of carriers and gradually form a dense layer of biofilm, reducing suspended particles and migrating membrane fouling (Bing et al., 2016). Moreover, BF-MBR can combine the advantages of both, controlling suspended particle concentration, reducing the energy cost and promoting the process efficiency (Duan et al., 2015a,b; Duan et al., 2015a,b).

Currently, most relevant research for BF-MBR (Duan et al., 2015a,b; Ivanovic and Leiknes, 2012) concentrate on pollutants removal and microbial community. In addition to pollutant degradation, membrane fouling is another significant factor affecting operational efficiency. In conventional activated sludge MBR, membrane fouling has been systematically studied (Lin et al., 2014; Wang et al., 2014). The membrane

* Corresponding author.

E-mail address: zhangwenxiang@gdut.edu.cn (W. Zhang).

foulants, such as soluble microbial products (SMP), polysaccharides, extracellular polymeric substances (EPS), humic acids and metal ions, were recognized (Lin et al., 2014; Meng et al., 2017). Some filtration and fouling theories, including critical flux (Pollice et al., 2005), porous media models (Yazdanshenas et al., 2010), mechanism of flow in capillary (Howell et al., 1993), resistance in series model (Naessens et al., 2012), polarization model (film theory (Yazdanshenas et al., 2005)), or classical fouling models (filtration laws and pore blocking model (Xiao et al., 2013)), were adopted to describe the membrane fouling mechanism of MBR. In theory, BF-MBR possesses a lower membrane fouling, thanks to lower suspended particle concentration. But, to our knowledge, to date, a comprehensive investigation about membrane fouling mechanism of BF-MBR has not been performed.

This paper encompasses a detailed investigation into fouling mechanism of BF-MBR. The effects of operational conditions including membrane types, agitation speed and TMP on flux behavior were studied. Then, pore blocking model were employed to explain membrane fouling process. Furthermore, the permeability recovery after membrane cleaning was utilized to investigate the irreversible fouling resistance and membrane cleaning efficiency. Besides operational testing, SEM was applied to observe and verify the microscopic morphology of cake layer on fouled membrane. In addition, an in-depth discussion for fouling mechanism was analyzed. The focus of this study is to understand on the fouling mechanism and to evaluate the membrane cleaning of BF-MBR, as well to facilitate its potential application to continuous filtration tests in the future.

2. Materials and methods

2.1. Materials

A moving bed bioreactor (MBBR) packed with bio-carrier (volumetric ratio of 32% (Vbio-carrier/Vreactor)) was used to carry out all the experiments. The used bioreactor was a cylindrical shape with a working volume of 27.7 L (50 × 30 cm). A circinate aeration trachea was evenly fixed under the frame to blow air bubbles for providing DO with a 23 h operational cycle and 1.5 L/min. During the whole experimental period, the hydraulic retention time (HRT) and the sludge retention time (SRT) were kept stably at 20 h and 30 d, respectively.

As show in Fig. 1, the effluent of MBBR flowed into membrane module. The test fluid for membrane experiment was the effluent of MBBR and its main characteristic was expressed in Table 1. Five fleet UF membranes fabricated by MICRODYN-NADIR GmbH were utilized for test in the present study. According to the manufacturer's information, their properties were listed in Table 2.

The dead-end filtration Amicon 8050 cell (Millipore, Billaica, USA)

Table 1
Main characteristics of test fluid.

COD (mg/L)	TP (mg/L)	NH ₄ -N (mg/L)	NO ₂ -N (mg/L)	NO ₃ -N (mg/L)	TSS (mg/L)	VSS (mg/L)
66.50	1.30	0.73	0.46	4.38	4121	3612

Table 2
Properties of MICRODYN-NADIR membranes tested.

Membrane	Surface material	Molecular weight cut-off (MWCO, kDa)	Water permeability (L m ⁻² h ⁻¹ bar ⁻¹) ^a
UP005	PES	5	10
UP010	PES	10	50
UP020	PES	20	65
UP030	PES	30	75
UP100	PES	100	100

PES, Polyethersulphone.

^a Own measurement at 20 °C.

was utilized in this investigation. As shown in Fig. 1, the internal diameter of the filtration cell is 6.35 cm and the maximum volume is 50 ml. The membrane was located at the bottom of the cell. The effective membrane area is 0.00317 m². A constant pressure was provided by filling the cell with nitrogen gas of nitrogen cylinder and the maximal pressure could reach 0.6 MPa, while permeate was collected in a tube placed on an electronic scale in order to calculate the permeate flux.

2.2. Experimental procedure

All experiments were conducted at a controlled room temperature of 20 °C. A new membrane was adopted for each test unless the permeability of the used membrane could be fully recovered to ensure the same initial membrane conditions for the entire study. The membranes were soaked in deionized water for at least 24 h before use, and pre-pressured with deionized water for 0.5 h under a pressure of 0.2 MPa. After stabilization, the pure water flux of membranes was measured at 0.2 MPa for UF to calculate water permeability (Lp). Before these experiments started, the feed was heated to 35 °C, and was fully recycled in the system at zero TMP, and this process lasted about 10 min for each test.

In the test, 50 mL of test fluid was concentrated at a constant pressure and the permeate flux was recorded with time, while permeate was not recycled. The first 20 mL of permeate was discarded. When another 30 mL permeate was obtained, the filtration was stopped and

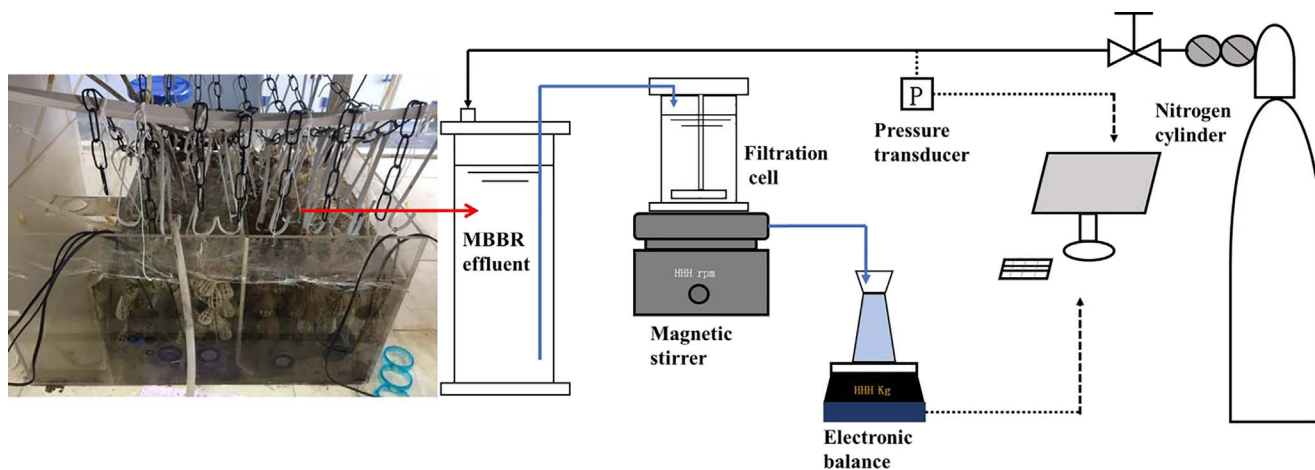


Fig. 1. Schematic diagram of the experimental configuration.

Table 3
Four models of membrane fouling proposed by Hermia.

Pore blocking models	Hermia's model	Physical concept	Schematic diagram
Complete pore blocking (model 1)	$J = J_0 \times \exp(-K \times t); K (s^{-1})$	Formation of a surface deposit	
Internal pore blocking (model 2)	$J = (J_0^{-0.5} + K \times t)^{-2}; K (m/s^2)$	Pore blocking + surface deposit	
Intermediate pore blocking (model 3)	$J = (J_0^{-1} + K \times t)^{-1}; K (m^{-1})$	Pore constriction	
Cake formation (model 4)	$J = (J_0^{-2} + K \times t)^{-0.5}; K (s/m^2)$	Pore blocking	

permeate were collected for the subsequent analysis.

After each series of tests, the filtration system was cleaned by deionized water for 10 min at 300 rpm. Then, alkaline cleaning was carried out by using a P3-ultrasil 10 (Ecolab, USA) detergent to remove foulants, at 0.25% concentration and 300 rpm, and L_p was measured to determine the permeability recovery.

2.3. Pore blocking model

In this study, the fouling type of BF-MBR process was identified by Hermia blocking model (Cancinomadariaga et al., 2012; Zhang et al., 2015a,b) (Table 3). The estimation of pore blocking coefficient (K -value) associated with each of the models could be calculated by non-linear regression of the experimental data.

Pore blocking model includes complete pore blocking, internal pore blocking, intermediate pore blocking and cake formation (Zhang and Ding, 2015). In complete pore blocking, all particles depositing on membrane surface only involve in “sealing” of membrane pores. It is an idealized condition assumes that no particles situated on top of other particles or on membrane surface. Internal pore blocking is due to constriction of membrane pores caused by small particles attached into pore walls. For intermediate pore blocking, each particle depositing on membrane not only cause pore blocking, but also attach on other particles on membrane surface. In the case of cake formation, particles do not participate in any changes of membrane pores. A cake layer forms outside the external membrane and increases hydraulic resistance.

2.4. Analytical items

General evaluation of the pollutant removal of BF-MBR was carried out by comparing the difference of the water quality indexes between the feed and the permeate. Regular parameters, including COD, NH_3-N , NO_2-N , NO_3-N , and TP were chosen as the reference parameters. All the above parameters were measured according to the standard methods (N°, 2006).

2.5. Membrane characterization

For the membranes before and after experiment, their morphologies were examined via scanning electron microscopy (SEM; SN-3400, Hitachi Ltd., Japan). The membrane weight was measured by means of an Electronic Scales (FA2004, China).

2.6. Calculated parameters

The rejection (R , %) was calculated according to the following equation:

$$R = \left(1 - \frac{C_p}{C_f}\right) \times 100\% \quad (1)$$

where C_p and C_f represented the water quality indexes in permeate and feed (average value during filtration process), respectively.

Water permeability (L_p) was calculated from:

$$L_p = \frac{J_w}{TMP} \quad (2)$$

where J_w is water permeate flux.

Permeability recovery was defined by a comparison of the average water permeability for cleaned and new membranes:

$$\text{Permeability recovery} = \frac{L_{pc}}{L_{pi}} \times 100\% \quad (3)$$

where L_{pc} and L_{pi} are water permeability ($L \text{ bar}^{-1} \text{ h}^{-1} \text{ m}^{-2}$) of the cleaned/fouled and new membranes, respectively.

Flux decline (FD) was calculated from:

$$\text{Fluxdecline (FD)} = \frac{J_i - J_f}{J_i} \times 100\% \quad (4)$$

where J_i and J_f are permeate flux at initial and finish time during the experiment, respectively.

2.7. Data analysis

All full recycling tests were repeated at least three times, and concentration tests were repeated at least two times. The errors were controlled below 5%. Mean values were calculated and presented on the Figures and Tables. Flux-time profile data were fitted to pore blocking model. The data were analyzed by nonlinear regression using Origin 8. Statistical analyses were undertaken through one-way ANOVA and significant differences for comparisons of treatment occurs if with $p < .05$.

3. Results and discussion

3.1. Effect of operating parameters on filtration behavior variation with time

The operating parameters, such as membrane type, shear rate and speed, impose a significant effect upon the flux behavior. In this section, the permeate flux and flux decline with time were studied.

3.1.1. Effect of membrane type on filtration behavior

Membrane module is the core of MBR (Zhang et al., 2015a,b). The selection of membrane type is very crucial for enhancing pollutant rejection and flux behavior, while alleviating membrane fouling (Fan et al., 2017a,b). Fig. 2 expresses the flux behavior variation with time

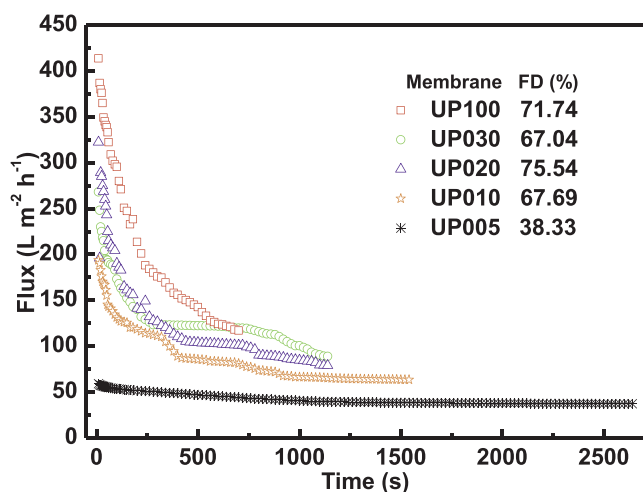


Fig. 2. Flux behaviors with time for different membranes (Agitation speed = 500 rpm and TMP = 0.25 MPa).

for five types of membranes. With the augment of membrane pore size and porosity, under the same agitation speed and TMP, the flux improved in the following order: UP005 < UP010 < UP020 < UP030 < UP100, in that larger pore size and greater porosity lead to lower inherent filtration resistance (Fan et al., 2017a,b). Due to larger pore size and greater porosity, the membrane with higher MWCO reveals lower inherent filtration resistance and higher flux. Moreover, more solutes and particles permeate through membrane pores at larger pore size, thus alleviating concentration polarization and foulants on membrane surface.

For all five membranes, they have similar changing tendencies and can be divided into three stages. At the first 250 s, flux reduced markedly. Between 250 s and 600 s, the flux decreased slowly. After 600 s, flux trended to be stable. At the first stage ($t < 250$ s), the foulants deposited and were adsorbed on membrane surface rapidly, so membrane fouling formed apparently and the flux reduced evidently. For the second stage ($250 < t < 600$ s), the fouling layer came into being and filtration resistance trended to be stable, thus the flux curtailed slightly. During the third stage ($t > 600$ s), the relationship between shear rate created by agitation speed and membrane fouling achieved the equilibrium, thus the flux reached a stable value. The fluxes in the first and the second stages are mainly determined by foulant-clean-membrane interaction, which depends on membrane properties (pore size, materials, etc.). With filtration continuation, the membrane fouling type changed from foulant-clean-membrane interaction to foulant-deposited interaction (Luo et al., 2011; Luo et al., 2012a,b,c). For the third stage, the main interaction effect between membrane and foulants trended to be foulant-deposited foulant interaction, so, their fluxes were close to each other and independent of membrane properties (foulant-deposited foulant interaction).

In Fig. 2, for all five UF membranes, their ending fluxes exceed $50 \text{ L m}^{-2} \text{ h}^{-1}$, which is much higher than the operational flux ($10\text{--}30 \text{ L m}^{-2} \text{ h}^{-1}$) of the conventional activated sludge MBR. This indicates that BF-MBR has a superior filtration efficiency and anti-fouling capacity to the conventional activated sludge MBR, although applying lab-scale results to full-scale plant operation may be limited due to certain differences in fouling rates and hydrodynamics. The design flux of BF-MBR can be much higher than that of the conventional activated sludge MBR, at the same time its fouling rate keeps at a low value. In addition, flux decline can also be observed in Fig. 2, according to Eq. (4), generally, higher initial flux has a higher flux decline. For UP005, its flux almost keeps stable for the whole test, thus its flux decline is only 38.33%. With respect to UP100, UP030, UP020 and UP010, their flux declines exceed 65%, due to their high initial flux and great flux reduction.

Table 4
Pollutant removal for different membranes (Agitation speed = 500 rpm and TMP = 0.25 MPa).

Pollutant rejection (%)	COD	TP	NH ₃ -N	NO ₂ -N	NO ₃ -N
UP100	93.01	99.40	97.92	97.50	99.78
UP030	93.61	99.40	97.50	97.50	99.71
UP020	93.50	99.55	97.75	97.66	99.73
UP010	93.65	99.36	97.58	97.66	99.74
UP005	93.71	99.32	94.08	98.28	99.84

Table 4 shows the pollutants rejection for COD, TP, NH₃-N, NO₂-N and NO₃-N. All five UF membranes have similar removal efficiency. COD removal rates vary from 92% to 94%. The removal rates of NH₃-N, NO₂-N, NO₃-N and TP exceed 96%. Overall, BF-MRB owns high pollutant removal efficiency. In theory, the membrane with larger pore size has a lower pollutant rejection, but the opposite occurs in this study, in that most pollutants in BF-MBR belong to large particles, which could be rejected by UF membranes. In addition, on the surfaces of all five membranes, foulants formed cake layers, which had a secondary rejection capacity, improving the rejection of pollutant particles. Compared with other membranes, the flux decline of UP030 is slightly lower, due to its excellent anti-fouling capacity produced by surface modification, and stable pollutant removal, therefore, it was selected for the following fouling mechanism study.

3.1.2. Effect of agitation speed and TMP on filtration behavior

Fig. 3 presents the effect of agitation speed on the filtration performance of BF-MBR effluent with the UP030 (0.25 mPa TMP). It is generally known that shear rate on membrane surface intensifies with higher agitation or rotating speed (Luo et al., 2010). As illustrated by Fig. 3, as expected, high shear rate could enhance turbulence near to membrane, decreasing solutes accumulation near membrane surface, thus alleviating concentration polarization and improving flux markedly, especially at high TMP. Besides, the shear-induced back diffusion enhanced at high shear rate, in particular of the large pollutant particles (size > 100 nm) (Luo et al., 2012a,b,c). Moreover, high shear rate also facilitated the recombination of some macro-pollutant particles (Luo et al., 2012a,b,c), which was conducive to shear-enhanced back transport. With decrease of agitation speed, at low shear rate, more foulants deposited on membrane and fouling resistance enhanced. Table 5 displayed the pollutants rejection for COD, TP, NH₃-N, NO₂-N and NO₃-N for different agitation speeds. As for the pollutant removal, the Table 5 shows that COD, NH₃-N, NO₂-N, NO₃-N and TP have highly similar rejection. All COD rejections are higher than 93%, and NH₃-N, NO₂-N,

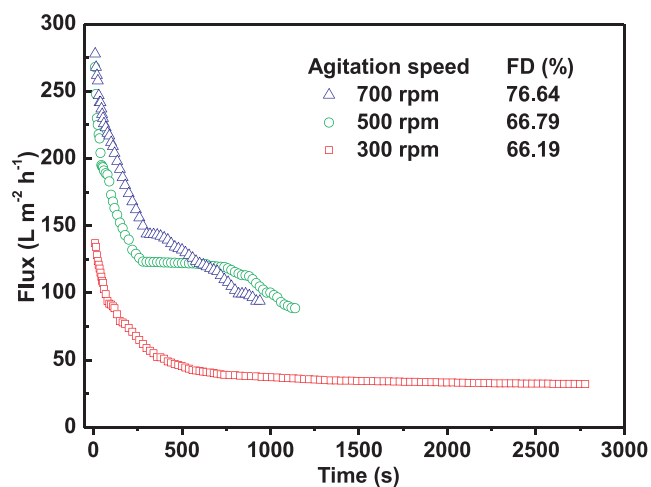


Fig. 3. Flux behaviors of UP030 with time for different agitation speeds (TMP = 0.25 MPa).

Table 5
Pollutant removal of UP030 with time for different agitation speeds (TMP = 0.25 MPa).

Pollutant rejection (%)	COD	TP	NH ₃ -N	NO ₂ -N	NO ₃ -N
700 rpm	95.28	99.47	97.33	97.19	99.76
500 rpm	95.40	98.80	97.75	97.34	99.93
300 rpm	95.46	99.51	97.08	97.81	99.82

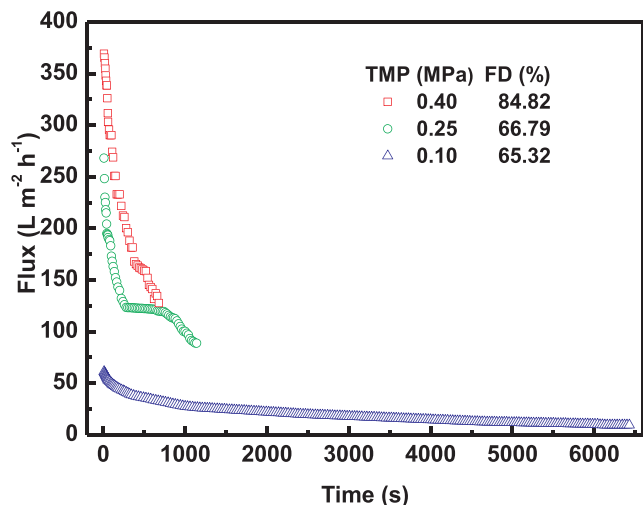


Fig. 4. Flux behaviors of UP030 with time for different TMPs (Agitation speed = 500 rpm).

NO₃-N and TP exceed 97%. Thus, the agitation speed imposes a minor effect upon pollutant separation. Therefore, it is concluded that a high shear rate on the membrane enables a reduction in fouling and produces a higher permeate flux.

Fig. 4 shows the effect of TMP on pollutant removal and permeability recovery after membrane cleaning with the UP030 (500 rpm agitation speed). In Section 3.1 and **Fig. 4**, as expected, TMP increases the driving force and improves flux. For the whole filtration test, high flux could shorten operational time, thus the operational time decreased with the following sequence: 0.40 MPa > 0.25 MPa > 0.10 MPa. Besides, higher TMP and high flux also promotes fouling resistances. At higher flux, more foulants were pushed onto membrane, leading to more serious foulants deposition and adsorption. In **Table 6**, the rejections of COD, NH₃-N, NO₂-N, NO₃-N and TP slightly decrease with TMP, implying that high TMP weakens the membrane rejection capacity. In membrane process, the flux could exert influence upon separation efficiency. In this case, flux increased with TMP, enhancing concentration gradient and diffusive effect transfer through the membrane, thus the transmission of pollutant particles enhanced.

3.2. Pore blocking coefficients and permeability recovery variations with changing operating parameters

In order to study the fouling mechanism of BF-MBR, four linear models of blocking model (complete pore blocking, internal pore blocking, intermediate pore blocking and cake layer) were utilized to analyze fouling process. For all the cases, the linear models were

Table 6
Pollutant removal of UP030 with time for different TMPs (Agitation speed = 500 rpm).

Pollutant rejection (%)	COD	TP	NH ₃ -N	NO ₂ -N	NO ₃ -N
0.10 MPa	95.40	98.80	97.75	97.34	99.93
0.25 MPa	95.46	99.51	97.08	97.81	99.82
0.40 MPa	95.10	99.17	98.17	97.03	99.89

Table 7
Pore blocking coefficients (K-value) and statistics analysis of fouling mechanism model for various membrane types.

Membrane	Model	R-squared	K-value	K-units
100k	1	0.4388	4.98E-06	s ⁻¹
	2	0.7909	3.88E+00	m/s ²
	3	0.9582	6.61E-03	m ⁻¹
	4	0.9944	7.47E-04	s/m ²
30k	1	0.3318	2.22E-06	s ⁻¹
	2	0.5833	1.79E+00	m/s ²
	3	0.7949	5.58E-03	m ⁻¹
	4	0.8838	1.36E-03	s/m ²
20k	1	0.9628	6.20E-07	s ⁻¹
	2	0.8816	2.43E+00	m/s ²
	3	0.8981	7.15E-03	m ⁻¹
	4	0.9735	1.57E-03	s/m ²
10k	1	0.9721	5.89E-07	s ⁻¹
	2	0.8959	1.87E+00	m/s ²
	3	0.9259	1.05E-02	m ⁻¹
	4	0.9624	5.47E-03	s/m ²
5k	1	0.9399	3.83E-07	s ⁻¹
	2	0.8417	6.61E-01	m/s ²
	3	0.8550	1.77E-02	m ⁻¹
	4	0.8789	6.10E-02	s/m ²

calculated by the experimental data from **Figs. 2–4** and the number of data points utilized in this work was sufficient for model fitting. The R-squares (**Table 7**) were used to evaluate the fitting degree of model and identify the type of pore blocking (**Zhang and Ding, 2015**). Highest R² value implies this model is most suitable to describe the fouling mechanism (**Cancinomadariaga et al., 2012**). As shown in **Tables 7–9**, the best fitting model for BF-MBR was cake formation model (0.9944 > R² > 0.8447). Thus, the primary fouling mechanism is cake formation pore blocking and the next one is intermediate pore blocking (0.9923 > R² > 0.7259). In some cases, the R-squares of models 1 and 2 exceed 96%, since complete pore blocking and internal pore blocking occur in these experiments. Therefore, cake formation pore blocking is the main fouling mechanism for this study, followed by intermediate pore blocking. This implies that most of fouled membrane areas were covered by cake layer, while for some parts of fouled membrane area, particles entered membrane pores and caused pore constriction. For the following investigations, a cake pore blocking coefficient k_b was applied to indicate the decrease of the membrane surface open to flow and membrane fouling degree. The pore blocking coefficients with various operating parameters are expressed in **Table 7**.

Table 8
Pore blocking coefficients (K-value) and statistics analysis of fouling mechanism model for various agitation speeds.

Agitation speed	Model	R-squared	K-value	K-units
300 rpm	1	0.9445	6.02E-07	s ⁻¹
	2	0.9686	2.41E+00	m/s ²
	3	0.9836	7.44E-03	m ⁻¹
	4	0.9839	1.26E-03	s/m ²
500 rpm	1	0.3318	2.22E-06	s ⁻¹
	2	0.5833	1.79E+00	m/s ²
	3	0.7949	5.58E-03	m ⁻¹
	4	0.8838	1.36E-03	s/m ²
700 rpm	1	0.9688	6.53E-07	s ⁻¹
	2	0.7053	1.52E+00	m/s ²
	3	0.7582	1.65E-02	m ⁻¹
	4	0.8447	2.28E-02	s/m ²

Table 9
Pore blocking coefficients (K-value) and statistics analysis of fouling mechanism model for various TMPs.

TMP	Model	R-squared	K-value	K-units
0.40 MPa	1	0.9445	4.53E-07	s ⁻¹
	2	0.6824	3.28E-01	m/s ²
	3	0.7258	1.93E-03	m ⁻¹
	4	0.8021	2.04E-03	s/m ²
0.25 MPa	1	0.3318	2.22E-06	s ⁻¹
	2	0.5833	1.79E+00	m/s ²
	3	0.7949	5.58E-03	m ⁻¹
	4	0.8838	1.36E-03	s/m ²
0.10 MPa	1	0.8928	1.16E-06	s ⁻¹
	2	0.9853	1.58E+00	m/s ²
	3	0.9923	6.32E-02	m ⁻¹
	4	0.9355	6.25E-01	s/m ²

3.2.1. Effect of membrane type on pore blocking coefficient and permeability recovery

In BF-MBR, the main foulants creating cake layer are large pollutant particles (size > 100 nm), including dissolved organic matters (DOMs), EPS and SMP. These foulants have a larger size than membrane pores, thus most foulants deposited on membrane surface, fouling layer formed, as well. With filtration continuation, with foulants accumulation, the thickness of fouling layer enhanced. For various membranes, as shown in Fig. 5, the cake pore blocking coefficient reduces with the membrane MWCO. Higher MWCO with higher membrane pore size and porosity has higher pollutants penetration rate, which could reduce foulants on membrane and alleviate concentration polarization, finally decrease foulants deposition and cake layer fouling. Besides, for the membrane of small pore size, its suspended particles on membrane surface had a complete particle diameter distribution, and its solute-membrane interaction included large particle-membrane and small particle-membrane. Therefore, the membrane with small pore size has a more compact and comprehensive solute-membrane interactions, as well as more serious cake layer.

Membrane cleaning efficiency is expressed by permeability recovery after physical cleaning, as displayed in Fig. 5. With the decrease of membrane pore size, the permeability of fouled membrane reduces, resulting from the high concentration polarization and fouling resistance, which is consistent with the above analysis. The whole membrane cleaning process includes physical cleaning and chemical cleaning. In physical cleaning, some “loose foulants” could be removed by water rinsing, thus their permeabilities were strengthened to varying degrees. Then, chemical cleaning (alkaline cleaning) were conducted adopting P3-ultrasil 10 (Ecolab, USA) detergent, which is a multi-

component detergent including EDTA, gluconate, phosphate, sulfate, NaOH and surfactant (Luo et al., 2012a,b,c). After chemical cleaning, some organic foulants, such as proteins and enzymes, and microbial foulants were removed, so permeability recovery promoted. Chemical cleaning could reinforce permeability recovery markedly. The explanation may be that: firstly, alkaline solution enlarged membrane swelling, penetrated the deep fouling position and took away the stubborn foulants; secondly, the organic foulants containing excess carboxyl reacted with alkaline solution and became negatively charged state, at the same time weakening the binding force between organic foulants and membrane materials, thus their solubility and molecular repulsion promoted; thirdly, the surfactants in ultrasil cleaning agents, which changed the interfacial tensions, could improve the solubilizing ability of cleaning agent, boost cleaning effect and enhance the hydrophilicity of membrane. Nevertheless, for all membranes, permeability could not be completely recovered, as some “stubborn foulants”, especially for the adsorption foulants into membrane pore wall, could not be effectively cleaned by P3-ultrasil 10. As for UP005, UP010 and UP020, their permeability recoveries of fouled membranes are lower than 85%, indicating that numerous foulants deposited on/into membrane, and serious cake layer occurred. Regarding UP030 and UP100, their permeability recovery are up to 93.5% and 97.2%, respectively, since they have low fouled degree and most of its foulants can be easily cleaned.

Besides, as shown in Fig. 5, there are two clear functional relationships ($k_b = 14.7MWCO^{-3.4}$) and permeability recovery = $97.07 - 24.15/(1 + e^{((MWCO - 23.23)/3.746)})$ for cake pore blocking coefficient-MWCO and permeability recovery-MWCO. Cake pore blocking coefficient has a power function with MWCO and permeability recovery after membrane cleaning has a positive correlation relationship with MWCO. Their R² values reach 0.9252 and 0.9985, respectively, thus exhibiting very high goodness of fit.

3.2.2. Effect of shear rate on pore blocking coefficient and permeability recovery

Fig. 6 and Table 8 plot k_b versus the agitation speed. k_b decreases with agitation speed. This result is in agreement with the fact that the high shear rate could curtail membrane fouling. This effect has two steps: firstly, high shear rate (Zhu et al., 2017) created by agitation speed produced a shear-induced diffusion for the larger foulant particles, therefore, it was difficult for foulants to deposit and agglomerate on membrane surface; secondly, high shear rate prevented the increase of the thickness of cake layer, implying that the enhancement of shear rate could clearly decrease the blocking membrane pores covered by cake layer which are not open to flow; thirdly, the higher shear rate improved the flux (Zhang et al., 2015a,b), reducing the contact time of membrane surface and foulants and their adsorption effect. Also, high

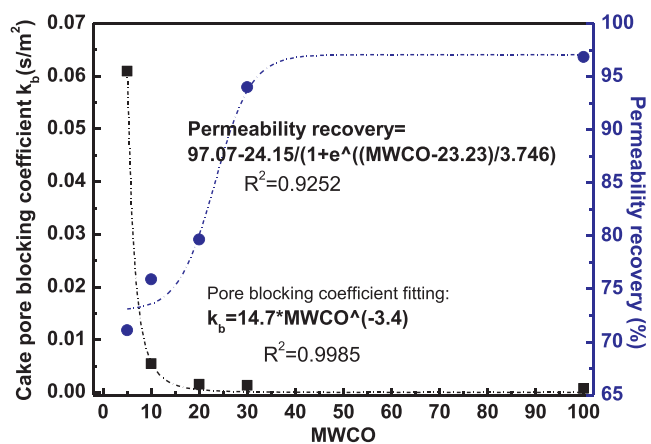


Fig. 5. Effect of membrane type on the cake pore blocking coefficient and permeability recovery (Agitation speed = 500 rpm and TMP = 0.25 MPa).

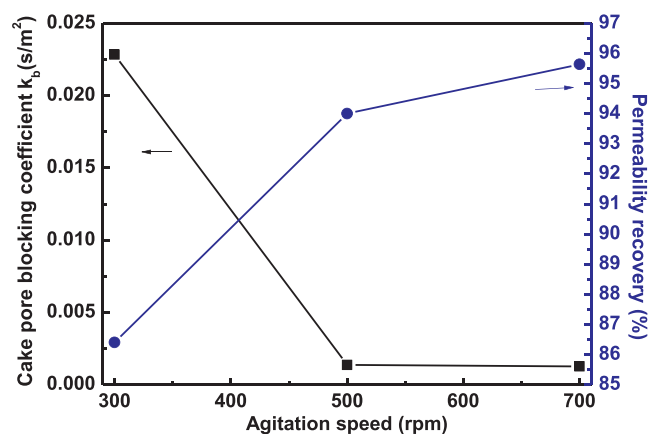


Fig. 6. Influence of agitation speed on the cake pore blocking coefficient and permeability recovery (TMP = 0.25 MPa and UP030).

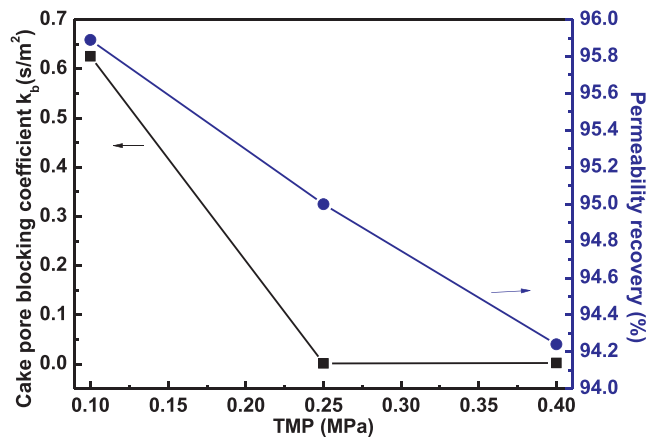


Fig. 7. Influence of TMP on the cake pore blocking coefficient and permeability recovery (Agitation speed = 500 rpm and UP030).

shear rate also facilitated the recombination of some macro-foulant particles (Luo et al., 2012a,b,c), which was conducive to shear-enhanced back transport. On the other hand, the permeability recovery improves with agitation speed, in that the raising shear rate helps reducing membrane fouling, specifically irreversible fouling, and promotes the cleaning efficiency.

3.2.3. Effect of TMP on pore blocking coefficient and permeability recovery

Fig. 7 and Table 9 show the influence of TMP on the cake pore blocking coefficient and permeability recovery. The cake pore blocking coefficient reduces with TMP, as higher flux at higher TMP exhibited shorter filtration process and decreased the contact time of foulants and membrane, thus alleviating pore blocking caused by cake layer. However, high TMP enhances irreversible fouling and reduces membrane cleaning efficiency. High TMP increased the driving force and strengthened concentration polarization, as well as compressed the foulants onto membrane surface, promoting the adsorption effect between foulants and membrane pores. In this case, the relationship between cake pore blocking and permeability recovery is not negatively correlated, implying that high cake layer does not necessarily enhance irreversible fouling.

It is obviously from the appearances of membrane surface, the new membrane surface is full of crackles and its membrane pores are clearly visible. Whereas other membranes appear white spots, which are membrane foulants, and their membrane pores narrow and are blurred. After filtration experiment at 0.25 MPa and 500 rpm, there was a white fouling layer formation on membrane surface, indicating the cake layer formation occurred on membrane surface. The thickness of membrane can be observed from the cross-section images. It includes the membrane surface layer and fouling layer. Compared with new membrane, as expected, the thickness enhanced significantly. Therefore, cake layer formation is the main fouling mechanism of BF-MBR.

3.3. Mini discussion

In this study, BF-MBR has a highly excellent flux behavior. In Fig. 2, all ending fluxes exceed $50 \text{ L m}^{-2} \text{ h}^{-1}$, which is much higher than the operational flux ($15\text{--}20 \text{ L m}^{-2} \text{ h}^{-1}$) of the conventional sludge MBR, thus, if BF-MBR is applied to engineering, its membrane fouling rate can always keep at a low level. Besides, as mentioned in Section 3.2, the thickness of cake layer and pore blocking coefficient are quite low. With suitable membrane cleaning, the permeability can be recovered up to 95%. Therefore, the membrane module of BF-MBR has excellent flux behavior.

From the mechanism, it can be explained as follows: in BF-MBR, the implementation of attached biofilm curtails the main foulants, including MLSS, SMP and EPS (Ivanovic and Leiknes, 2012). At the same

time, the carriers can flocculate suspended biomass and promote formation of larger flocs (Duan et al., 2015a,b), thus improving the physical properties (i.e., particle size and viscosity) and reducing fouling rates.

In this investigation, Hermia pore blocking models were adopted to assess the membrane fouling in BF-MBR. Compared with other four membranes, UP030 with high permeate flux, low flux decline and stable pollutant removal was selected for the following fouling mechanism study. Increasing agitation speed and TMP, and selecting suitable membrane type enhanced flux behavior, but had limiting effect on pollutant removal. The experimental data was in agreement with the cake formation model, implying that the primary fouling mechanism of BF-MBR was cake layer occurring during BF-MBR filtration process. Intermediate pore blocking was the second fouling mechanism. This implies that most of fouled membrane areas were covered by cake layer, while for some parts of fouled membrane area, particles entered membrane pores and caused pore constriction. The cake pore blocking coefficients of Hermia were utilized to evaluate the degree of membrane fouling. High agitation speed and TMP, and selecting the membrane with large MWCO could curtail cake blocking fouling. Then, water rinse and chemical cleaning were employed to clean fouled membrane. The permeability recoveries improved with the increment of agitation speed and the decrement of TMP. In addition, here is an interesting fitting phenomenon: both cake pore blocking coefficient and permeability recovery had a highly fitting relationship with membrane MWCO. These findings not only clarify the fouling mechanism of BF-MBR, but also provide valuable advice for membrane cleaning in MBR operations.

4. Conclusion

In this investigation, Hermia pore blocking models were adopted to assess the membrane fouling in BF-MBR. The primary fouling mechanism of BF-MBR was cake layer occurring during BF-MBR filtration process. Compared with other four membranes, UP030 with high permeate flux, low flux decline and stable pollutant removal was selected for the following fouling mechanism study. Increasing agitation speed and TMP, and selecting suitable membrane type enhanced flux behavior, but had limiting effect on pollutant removal. These findings not only clarify the fouling mechanism of BF-MBR, but also provide valuable advice for membrane cleaning in MBR operations.

Acknowledgements

The authors would like to acknowledge the financial support from the National Natural Science Foundation of China (No. 41371473), Guangdong Natural Science Foundation of China (No. 2017A030310540), Guangdong provincial education department Youth Innovative Talents Project (No. 17ZK0110), Scientific Research Fund of Guangdong University of Technology (No. 220413582), and National Natural Science Foundation of China (No. 21476050).

Appendix A. Supplementary data

Supplementary data associated with this article can be found, in the online version, at <http://dx.doi.org/10.1016/j.biortech.2017.11.036>.

References

- Bassin, J.P., Kleerebezem, R., Rosado, A.S., Loosdrecht, M.C.M.V., Dezotti, M., 2012. Effect of different operational conditions on biofilm development, nitrification, and nitrifying microbial population in moving-bed biofilm reactors. *Environ. Sci. Technol.* 46, 1546–1555.
- Bing, T., Yu, C., Bin, L., Zhao, Y., Feng, X., Huang, S., Fu, F., Ding, J., Chen, C., Ping, L., 2016. Essential factors of an integrated moving bed biofilm reactor–membrane bioreactor: adhesion characteristics and microbial community of the biofilm. *Bioresour. Technol.* 211, 574–583.

- Cancinomadariaga, B., Ruby, R., Castro, C.A., Torrico, J.S., Riquelme, M.L., 2012. Analysis of the membrane fouling mechanisms involved in clarified grape juice ultrafiltration using statistical tools. *Ind. Eng. Chem. Res.* 51, 4017–4024.
- Duan, L., Li, S., Han, L., Song, Y., Zhou, B., Zhang, J., 2015a. Comparison between moving bed-membrane bioreactor and conventional membrane bioreactor systems. Part I: membrane fouling. *Environ. Earth Sci.* 73, 4881–4890.
- Duan, L., Tian, Y., Liu, X., Song, Y., Yang, L., Zhang, J., 2015b. Comparison between moving bed-membrane bioreactor and conventional membrane bioreactor systems. Part II: bacterial community. *Environ. Earth Sci.* 73, 4891–4902.
- Fan, J., Luo, J., Wan, Y., 2017a. Aquatic micro-pollutants removal with a biocatalytic membrane prepared by metal chelating affinity membrane chromatography. *Chem. Eng. J.*
- Fan, J., Luo, J., Wan, Y., 2017b. Membrane chromatography for fast enzyme purification, immobilization and catalysis: a renewable biocatalytic membrane. *J. Membr. Sci.*
- Fenu, A., Guglielmi, G., Jimenez, J., Spèrandio, M., Saroj, D., Lesjean, B., Brepols, C., Thoeue, C., Nopens, I., 2010. Activated sludge model (ASM) based modelling of membrane bioreactor (MBR) processes: a critical review with special regard to MBR specificities. *Water Res.* 44, 4272–4294.
- Howell, J.A., Sanchez, V., Field, R.W., 1993. *Membranes in Bioprocessing: Theory and Applications*.
- Huang, L., Lee, D.J., 2015. Membrane bioreactor: a mini review on recent R&D works. *Bioresour. Technol.* 194, 383.
- Ivanovic, I., Leiknes, T.O., 2012. The biofilm membrane bioreactor (BF-MBR)—a review. *Desalin. Water Treat.* 37, 288–295.
- Leiknes, T.O., Ødegaard, H., 2007. The development of a biofilm membrane bioreactor. *Desalination* 202, 135–143.
- Leyva-Díaz, J.C., Martín-Pascual, J., Muñío, M.M., González-López, J., Hontoria, E., Poyatos, J.M., 2014. Comparative kinetics of hybrid and pure moving bed reactor-membrane bioreactors. *Ecol. Eng.* 70, 227–234.
- Lin, H., Zhang, M., Wang, F., Meng, F., Liao, B.Q., Hong, H., Chen, J., Gao, W., 2014. A critical review of extracellular polymeric substances (EPSs) in membrane bioreactors: characteristics, roles in membrane fouling and control strategies. *J. Membr. Sci.* 460, 110–125.
- Luo, J.Q., Ding, L.H., Wan, Y.H., Paullier, P., Jaffrin, M.Y., 2010. Application of NF-RDM (nanofiltration rotating disk membrane) module under extreme hydraulic conditions for the treatment of dairy wastewater. *Chem. Eng. J.* 163, 307–316.
- Luo, J., Ding, L., Qi, B., Jaffrin, M.Y., Wan, Y., 2011. A two-stage ultrafiltration and nanofiltration process for recycling dairy wastewater. *Bioresour. Technol.* 102, 7437–7442.
- Luo, J., Ding, L.H., Wan, Y., Paullier, P., Jaffrin, M.Y., 2012c. Fouling behavior of dairy wastewater treatment by nanofiltration under shear-enhanced extreme hydraulic conditions. *Sep. Purif. Technol.* 88, 79–86.
- Luo, J., Ding, L., Wan, Y., Jaffrin, M.Y., 2012b. Threshold flux for shear-enhanced nanofiltration: experimental observation in dairy wastewater treatment. *J. Membr. Sci.* 409–410, 276–284.
- Luo, J., Ding, L., Wan, Y., Jaffrin, M.Y., 2012a. Flux decline control in nanofiltration of detergent wastewater by a shear-enhanced filtration system. *Chem. Eng. J.* 181–182, 397–406.
- Luostarinen, S., Luste, S., Valentín, L., Rintala, J., 2006. Nitrogen removal from on-site treated anaerobic effluents using intermittently aerated moving bed biofilm reactors at low temperature. *Water Res.* 40, 1607–1615.
- Meng, F., Zhang, S., Oh, Y., Zhou, Z., Shin, H.S., Chae, S.R., 2017. Fouling in membrane bioreactors: an updated review. *Water Res.* 114, 151.
- Naessens, W., Maere, T., Ratkovich, N., Vedantam, S., Nopens, I., 2012. Critical review of membrane bioreactor models—part 2: hydrodynamic and integrated models. *Bioresour. Technol.* 122, 107–118.
- Ng, A.N.L., Kim, A.S., 2007. A mini-review of modeling studies on membrane bioreactor (MBR) treatment for municipal wastewaters. *Desalination* 212, 261–281.
- N^o, 2006. *Standard Methods for the Examination of Water and Wastewater, twentyfirst Edition*. Journal – American Water Works Association, 130.
- Pollice, A., Brookes, A., Jefferson, B., Judd, S., 2005. Sub-critical flux fouling in membrane bioreactors—a review of recent literature. *Desalination* 174, 221–230.
- Wang, Z., Ma, J., Tang, C.Y., Kimura, K., Wang, Q., Han, X., 2014. Membrane cleaning in membrane bioreactors: a review. *J. Membr. Sci.* 468, 276–307.
- Xiao, K., Shen, Y., Huang, X., 2013. An analytical model for membrane fouling evolution associated with gel layer growth during constant pressure stirred dead-end filtration. *J. Membr. Sci.* 427, 139–149.
- Yazdandshenas, M., Tabatabaeezad, A.R., Roostaazad, R., Khoshfetrat, A.B., 2005. Full scale analysis of apple juice ultrafiltration and optimization of diafiltration. *Sep. Purif. Technol.* 47, 52–57.
- Yazdandshenas, M., Soltanieh, M., Nejad, S.A.R.T., Fillaudeau, L., 2010. Cross-flow microfiltration of rough non-alcoholic beer and diluted malt extract with tubular ceramic membranes: investigation of fouling mechanisms. *J. Membr. Sci.* 362, 306–316.
- Zhang, W., Ding, L., 2015. Investigation of membrane fouling mechanisms using blocking models in the case of shear-enhanced ultrafiltration. *Sep. Purif. Technol.* 141, 160–169.
- Zhang, W., Grimi, N., Jaffrin, M.Y., Ding, L., 2015a. Leaf protein concentration of alfalfa juice by membrane technology. *J. Membr. Sci.* 489, 183–193.
- Zhang, W., Liang, W., Huang, G., Wei, J., Ding, L., Jaffrin, M.Y., 2015b. Studies of membrane fouling mechanisms involved in the micellar-enhanced ultrafiltration using blocking models. *RSC Adv.* 5, 48484–48491.
- Zhu, Z., Wu, Q., Di, X., Li, S., Barba, F.J., Koubaa, M., Roohinejad, S., Xiong, X., He, J., 2017. Multistage recovery process of seaweed pigments: investigation of ultrasound assisted extraction and ultra-filtration performances. *Food Bioprod. Process.* 104.